2024 IEEE/RSJ International Conference on Intelligent Robots and Systems (IROS)
October 14-18, 2024. Abu Dhabi, UAE

Modelling and Analysis of Joint-to-End Variable Stiffness for Cable-Driven Hyper-Redundant Manipulator

Hongyang Zhang, Shuting Wang, Hu Li, *IEEE*, *Member*,
Yuanlong Xie, *IEEE*, *Senior Member*

***Abstract*— To ensure operational accuracy and flexibility in confined environments, the cable-driven hyper-redundant manipulator needs to take into account both compliance and stiffness. Although the cable-driven method enables the manipulator to have adjustable stiffness, the theoretical analyses and studies on the effects of various factors on the stiffness are insufficient, leading to the possibility that the existing variable stiffness strategies may disrupt the equilibrium state of the manipulator. Accordingly, this paper presents the modeling and analysis of joint-to-end variable stiffness for cable-driven hyper-redundant manipulator. First, the multi-layered static models are constructed to decouple and characterise the complex robotic arm system by combining the manipulator kinematics with the virtual work principle. Then, the joint-to-end analytical stiffness models are developed to explore the influencing factors of stiffness, and relevant stiffness indicators are designed to evaluate the stiffness level. Finally, with platform validation and numerical method, the connections between cable tension, joint angle, joint stiffness and end stiffness are analysed, thereby summarising the variable stiffness characteristics of the cable-driven super-redundant manipulator.**

I. INTRODUCTION

The cable-driven hyper-redundant manipulator has the characteristics of self-supporting ability, slender physique and multiple degrees of freedom [1]–[3]. Compared with the traditional manipulators, the utilization of cables to drive each joint endows the hyper-redundant manipulator with flexibility with obstacle avoidance proficiency in confined spaces and adaptability in challenging environments, as shown in Fig. 1. Nevertheless, during task execution, the manipulator requires high stiffness to enhance the end-effector's precise positioning and bearing capacity. Consequently, the cable-driven hyper-redundant manipulator necessitates variable stiffness characteristics to meet diverse task demands. This has garnered the interest of numerous domestic and international institutions [4], [5].

Existing conventional methods use variable stiffness actuator (VSA) to adjust the stiffness, which are mainly used in traditional manipulators [6], [7]. However, for cable-driven hyper-redundant manipulator, the VSA can increase their load and even affect operational performance. At present, it is also proposed to use pneumatic muscle actuators [8], [9], shape memory materials [10], [11] and temperature-related materials [12] to achieve variable stiffness control for soft manipulators, but these methods will increase the cost and complexity of the system. In addition, antagonistic actuation by varying the cable tensions is an effective way to actively strengthen the stiffness of parallel robots [13], [14]. Due to its simplistic control, this method is currently applied to cable-driven super-redundant manipulator. However, these methods regulate the stiffness by dynamically controlling the cable tensions, which may affect the static balance of the manipulator and even the end pose error [15], [16]. Meanwhile, the motion of the end-effector requires the cooperation of multiple groups of cables, which drive the corresponding joints. Nevertheless, it is difficult to measure the effect of each group of cables on the end stiffness using the system model constructed by these methods. For hyper-redundant manipulator, its overall configuration also affects the end stiffness. Existing method achieves variable stiffness by optimally solving the inverse kinematics, and does not analyse the influence of joint angles on the stiffness [17]. Therefore, the current methods for achieving variable stiffness of cable-driven hyper-redundant manipulator are still inadequate in terms of theoretical analysis and research.

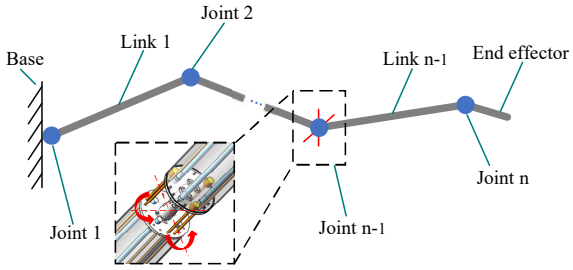

Fig. 1. The structural diagram of rope-driven hyper-redundant manipulator.

Inspired by these observations, we propose a new modelling and analysis method of joint-to-end variable stiffness for cable-driven hyper-redundant manipulator. It is used to analyse the coupling mechanism between cable tension, joint angle, joint stiffness and end stiffness. The main contributions of this paper are summarized as follows: 1) The multi-layered static models of cable-joint and joint-end are constructed respectively to decouple the complex system model; 2) We derive the joint-to-end stiffness models that are employed to analyse the controllable factors affecting the stiffness, and then establish the performance indicators of the variable stiffness to characterise the adjustable levels of joint

*The work was supported by National Natural Science Foundation of China under Grant 52275488, Key Research and Development Program of Hubei Province, China under Grant 2022BAA064 and Key Research and Development Program of Henan Province, China under Grant 221111220800 (Corresponding author: Yuanlong Xie)

Hongyang Zhang, Shuting Wang, Hu Li, Yuanlong Xie are with School of Mechanical Science and Engineering, Huazhong University of Science and Technology, Wuhan 430074, China (e-mail: hongyang, wangst, lihu, yuanlongxie@hust.edu.cn)

stiffness and end stiffness; 3) Through platform validation and numerical method, it analyses the effects of cable tension and joint angle on the joint stiffness, and the connection between the joint stiffness and the end stiffness. Through the analysis and summary, this paper can provide a theoretical basis for the subsequent research on deformation compensation, variable stiffness control, and flexibility control.

The rest of the paper is organised as follows: Section II describes the construction method of static model. Section III establishes the stiffness models of the joint and end, and designs the performance indicators. The factors affecting the stiffness are analysed in Section IV. Finally, the conclusions are provided in Sections V.

II. STATICS MODELLING

For the cable-driven hyper-redundant manipulator, constructing static models is the basis for investigating their stiffness problems. In this section, the statics are analysed in conjunction with the existence of multi-coupling positional relationships between cable, joint and end.

A. Cable-joint Static Model

Using a 3-cable 2-*DOF* single joint as the object of research, while ignoring the deformation of the cable due to gravity and the friction between the cable and hole. The pose transformation of the joint can be clearly depicted in Fig. 2. The i-th joint base coordinate system O_i and the transformation coordinate system O_i' are set up respectively. The pose transformation between the two coordinate systems can be described as follows:

$$\begin{aligned}\boldsymbol{R} = &\text{Trans}(0,0,d_{i,1}) \cdot \text{Rot}(x, q_{i,1}) \cdot \text{Rot}(y, q_{i,2}) \\ &\cdot \text{Trans}(0,0,d_{i,2})\end{aligned} \tag{1}$$

where $q_{i,1}$ and $q_{i,2}$ denote the i-th joint angles, and $d_{i,1}$ and $d_{i,2}$ denote the displacements.

According to the vector loop equation, the relationship between the pose transformation and the cable length is:

$$l_{i,j} = r_j - \boldsymbol{R} \cdot r_j' \tag{2}$$

where l_j denotes the j-th cable vector from H_j to H_j', r_j denotes the position vector of H_j in O_i, $r_j + 1$ denotes the position vector of H_j' 'in O_i', and $j = 1, 2, 3$.

The relationship between the velocity vectors of the cables and joint angle via the differentiation of (2) with respect to time can be obtained. Furthermore, the angular virtual displacement $\delta \boldsymbol{q}$ and the cable length virtual displacement $\delta \boldsymbol{l}$ satisfy the relationship as follows:

$$\delta \boldsymbol{l} = \boldsymbol{J_c} \cdot \delta \boldsymbol{q} \tag{3}$$

where $\boldsymbol{J_c} \in R^{3\times 2}$ is the Jacobi matrix of the cable-joint.

According to the principle of virtual displacement, it can be obtained that the virtual work done by the cable tensions is equal to the virtual work done by the joint torques.

$$\boldsymbol{f}^T \cdot \delta \boldsymbol{l} + \boldsymbol{\tau}^T \cdot \delta \boldsymbol{q} = 0 \tag{4}$$

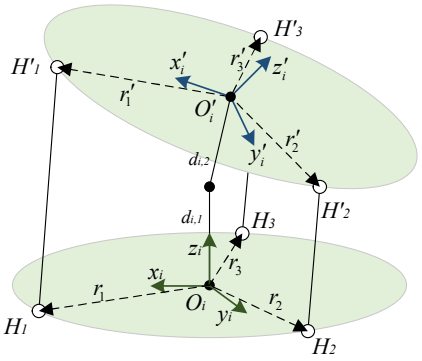

Fig. 2. The structural diagram of the cable-joint connection.

where $\boldsymbol{f} = [f_{i,1}, f_{i,2}, f_{i,3}]^T$ denotes the cable tensions and $\boldsymbol{\tau} = [\tau_{i,1}, \tau_{i,2}]^T$ denotes the joint torques.

The cable-joint static model can be obtained by substituting (3) into (4).

$$\boldsymbol{\tau} = -\boldsymbol{J_c^T} \cdot \boldsymbol{f} \tag{5}$$

B. Joint-end Static Model

For the $2n$-*DOF* hyper-redundant manipulator with forward kinematic map, the robot is assumed to be in equilibrium state [18] when its joint angle is $\boldsymbol{Q}_0 = [q_1, q_2 \dots q_{2n}]^T$. Its equilibrium state $\boldsymbol{M}_0$ can be expressed as:

$$\boldsymbol{M}_0 = \boldsymbol{T}_0 - \boldsymbol{J}_x^T(\boldsymbol{Q}_0)\boldsymbol{F}_0 - \boldsymbol{T}_g(\boldsymbol{Q}_0) = 0 \tag{6}$$

where $\boldsymbol{T}_0 = [\tau_1, \tau_2 \dots \tau_{2n}]^T$ denotes the torque of all joints in static equilibrium, $\boldsymbol{F}_0$ denotes the external force applied to the end, and $\boldsymbol{T}_g$ denotes the gravity vector. $\boldsymbol{J}_x^T \in R^{6\times 2n}$ denotes the Jacobi matrix of the joint-end of the manipulator, x denotes the end pose.

The equilibrium point $\boldsymbol{M}$ in the neighbourhood of setting $\boldsymbol{M}_0$ exists, and is defined as:

$$\begin{aligned}\boldsymbol{M} =&\boldsymbol{T}_0 + \delta\boldsymbol{T} - \boldsymbol{J}_x^T(\boldsymbol{Q}_0 + \delta\boldsymbol{Q})(\boldsymbol{F}_0 + \delta\boldsymbol{F}) \\ &- \boldsymbol{T}_g(\boldsymbol{Q}_0 + \delta\boldsymbol{Q})) = 0\end{aligned} \tag{7}$$

where $\boldsymbol{T}_0 = [\tau_1, \tau_2 \dots \tau_{2n}]^T$ denotes the torque of all joints in static equilibrium, $\boldsymbol{F}_0$ denotes the external force applied to the end, and $\boldsymbol{T}_g$ denotes the gravity vector. $\boldsymbol{J}_x^T \in R^{6\times 2n}$ denotes the Jacobi matrix of the joint-end of the manipulator, x denotes the position/orientation of the end.

By taking a first-order Taylor expansion, (7) is written as:

$$\begin{aligned}\boldsymbol{M} \approx&\boldsymbol{T}_0 + \delta\boldsymbol{T} - \boldsymbol{J}_x^T(\boldsymbol{Q}_0)\boldsymbol{F}_0 - \left.\frac{\partial \boldsymbol{J}_x^T(\boldsymbol{Q})\boldsymbol{F}_0}{\partial \boldsymbol{Q}}\right|_{\boldsymbol{Q}_0} \delta\boldsymbol{Q} \\ &- \boldsymbol{J}_x^T(\boldsymbol{Q}_0)\delta\boldsymbol{F} - \left.\frac{\partial \boldsymbol{J}_x^T(\boldsymbol{Q})\delta\boldsymbol{F}}{\partial \boldsymbol{Q}}\right|_{\boldsymbol{Q}_0,\boldsymbol{F}_0} \delta\boldsymbol{Q} \\ &- \boldsymbol{T}_g(\boldsymbol{Q}_0) - \left.\frac{\partial \boldsymbol{T}_g(\boldsymbol{Q}_0)}{\partial \boldsymbol{Q}}\right|_{\boldsymbol{Q}_0} \delta\boldsymbol{Q} = 0\end{aligned} \tag{8}$$

For the final gravity term, the Jacobi matrix $\boldsymbol{J}_h^T(\boldsymbol{Q})$ for the mass centres of links and joints are introduced. Combined with (6) (8), the joint-end static model can be obtained:

$$\begin{cases} \delta \boldsymbol{T} - \boldsymbol{J}_x^T(\boldsymbol{Q}_0)\delta \boldsymbol{F} - \boldsymbol{W} = 0 \\ \boldsymbol{W} = \dfrac{\partial \boldsymbol{J}_x^T(\boldsymbol{Q})\boldsymbol{F}_0}{\partial \boldsymbol{Q}}\Big|_{\boldsymbol{Q}_0} \delta \boldsymbol{Q} + \sum_{i=1}^{2n} \dfrac{\partial \boldsymbol{J}_{h,i}^T(\boldsymbol{Q})\boldsymbol{G}_i}{\partial \mathbf{Q}}\Big|_{\boldsymbol{Q}_0} \delta \boldsymbol{Q} \end{cases} \tag{9}$$

where $\boldsymbol{G}_i$ is the gravity vector of the i-th link or joint.

III. STIFFNESS MODELS AND INDICATORS

A. Joint Stiffness

The anti-deformation ability of the system under external force can be used to measure its stiffness level. Hence, it can be expressed as the relationship between a small torque $\delta \boldsymbol{\tau}$ acting on the joint and a small change $\delta \boldsymbol{q}$ of the joint angle.

$$\delta \boldsymbol{\tau} = \boldsymbol{K}_c \cdot \delta \boldsymbol{q} \tag{10}$$

where $\boldsymbol{K}_c$ denotes the joint stiffness matrix. For a given joint angle $\boldsymbol{q}$, the joint stiffness is assumed to be locally linear.

Combined with (5) (10), the stiffness matrix $\boldsymbol{K}_c$ of a single joint can be obtained:

$$\boldsymbol{K}_c = \frac{\partial \boldsymbol{\tau}}{\partial \boldsymbol{q}} = -\left(\frac{\partial \boldsymbol{J}_c^T}{\partial \boldsymbol{q}} \boldsymbol{f} + \boldsymbol{J}_c^T \frac{\partial \boldsymbol{f}}{\partial \boldsymbol{q}} \right) \tag{11}$$

It can be seen from (11) that the system stiffness matrix consists of two parts. $\frac{\partial \boldsymbol{J}_c^T}{\partial \boldsymbol{q}} \boldsymbol{f}$ can be controlled by changing the cable tension, which is called controllable stiffness. Combined with (3), $\boldsymbol{J}_c^T \frac{\partial \boldsymbol{f}}{\partial \boldsymbol{q}}$ can be transformed as follows:

$$\boldsymbol{J}_c^T \frac{\partial \boldsymbol{f}}{\partial \boldsymbol{q}} = \boldsymbol{J}_c^T \frac{\partial \boldsymbol{f}}{\partial \boldsymbol{l}} \frac{\partial \boldsymbol{l}}{\partial \boldsymbol{q}} = \boldsymbol{J}_c^T \frac{\partial \boldsymbol{f}}{\partial \boldsymbol{l}} \boldsymbol{J}_c \tag{12}$$

where $\frac{\partial \boldsymbol{f}}{\partial \boldsymbol{l}}$ is cable stiffness. For three cables, their stiffness are determined by their own physical properties. Therefore, this item is called inherent stiffness. The cable stiffness $\boldsymbol{K}_l$ can be expressed as follows:

$$\boldsymbol{K}_l = \frac{\partial \boldsymbol{f}}{\partial \boldsymbol{l}} = diag\left(\frac{E_1 \cdot A_1}{l_1}, \frac{E_2 \cdot A_2}{l_2}, \frac{E_3 \cdot A_3}{l_3} \right) \tag{13}$$

where *E*, *A* and *l* are the elastic modulus, cross-sectional area and length of the cable, respectively.

Thus, (11) can be expressed as:

$$\boldsymbol{K}_c = \frac{\partial \boldsymbol{\tau}}{\partial \boldsymbol{q}} = -\frac{\partial \boldsymbol{J}_c^T}{\partial \boldsymbol{q}} \boldsymbol{f} - \boldsymbol{J}_c^T \boldsymbol{K}_l \boldsymbol{J}_c \tag{14}$$

At a defined joint angle and cable stiffness, it can be demonstrated that changes in joint stiffness can be achieved by adjusting the tension.

B. End Stiffness

Similar to joint stiffness, it can be concluded that the relationship between a small external force $\delta \boldsymbol{F}$ acting on the end-effector and a small change $\delta \boldsymbol{x}$ of the end pose.

$$\delta \boldsymbol{F} = \boldsymbol{K}_x \cdot \delta \boldsymbol{x} \tag{15}$$

where $\boldsymbol{K}_x$ denotes the end stiffness matrix. To derive $\boldsymbol{K}_x$, the joint-end static model (9) can be transformed:

$$\frac{\delta \boldsymbol{Q}}{\delta \boldsymbol{F}} = \left[\frac{\delta \boldsymbol{T}}{\delta \boldsymbol{Q}} - \frac{\boldsymbol{W}}{\delta \mathbf{Q}} \right]^{-1} \boldsymbol{J}_x^T(\boldsymbol{Q}_0) \tag{16}$$

Also, $\frac{\delta \boldsymbol{Q}}{\delta \boldsymbol{F}}$ can be expressed through kinematic relationship.

$$\frac{\delta \boldsymbol{Q}}{\delta \boldsymbol{F}} = \frac{\delta \boldsymbol{Q}}{\delta \boldsymbol{x}} \frac{\delta \boldsymbol{x}}{\delta \boldsymbol{F}} = \left(\boldsymbol{J}_x(\mathbf{Q_0}) \right)^{-1} \frac{\delta \boldsymbol{x}}{\delta \boldsymbol{F}} \tag{17}$$

Combining (16) (17), it can be obtained:

$$\left(\frac{\delta \mathbf{F}}{\delta \mathbf{x}} \right)^{-1} = \boldsymbol{J}_x(\boldsymbol{Q}_0) \left[\frac{\delta \boldsymbol{T}}{\delta \boldsymbol{Q}} - \frac{\boldsymbol{W}}{\delta \mathbf{Q}} \right]^{-1} \boldsymbol{J}_x^T(\boldsymbol{Q}_0) \tag{18}$$

where $\frac{\delta \boldsymbol{T}}{\delta \boldsymbol{Q}}$ denotes the total stiffness matrix of the joint $\boldsymbol{K}_q$. Combined with the single joint stiffness (14), it can be expressed as $\boldsymbol{K}_q = diag(\boldsymbol{K}_{c,1}, \boldsymbol{K}_{c,2}, \cdots \boldsymbol{K}_{c,n})$. Further, the end stiffness can be solved by combining (15) (18).

$$\boldsymbol{K}_x^{-1} = \boldsymbol{J}_x(\boldsymbol{Q}_0) \left[\boldsymbol{K}_q - \frac{\boldsymbol{W}}{\delta \mathbf{Q}} \right]^{-1} \boldsymbol{J}_x^T(\boldsymbol{Q}_0) \tag{19}$$

From (19), it can be concluded that changing the joint stiffness $\boldsymbol{K}_q$ can effectively control the end stiffness. Meanwhile, by adjusting the joint angles, the Jacobi matrix $\boldsymbol{J}_x^T$ can also be modified to achieve the end stiffness adjustment.

Through the above derivation, the relationship between tension, joint stiffness and end stiffness can be established, thereby providing a theoretical basis for subsequent analysis of variable stiffness characteristics.

C. Stiffness Indicators

To characterise the level of joint stiffness and end stiffness, stiffness indicators are designed separately, which include:

1) Joint stiffness magnitude and range: define the the stiffness magnitude of the *i*-joint along the x-axis and y-axis as $K_{i,x}$, $K_{i,y}$. For the single joint stiffness matrix $\boldsymbol{K}_c = [K_{11}, K_{12}; K_{21}, K_{22}]$, $K_{i,x}$ and $K_{i,y}$ correspond to K_{11} and K_{22} of the matrix, respectively.

Define $K_{i,x} \in [K_{i,x}^{\min}, K_{i,x}^{\max}]$ and $K_{i,y} \in [K_{i,y}^{\min}, K_{i,y}^{\max}]$, The variation ranges of joint stiffness can be expressed as $\Delta k_{i,x} = K_{i,x}^{\max} - K_{i,x}^{\min}$, $\Delta k_{i,y} = K_{i,y}^{\max} - K_{i,y}^{\min}$. Therefore, The index of joint stiffness can be defined as:

$$\begin{cases} \boldsymbol{\sigma}_{i,x} = [K_{i,x}, \Delta k_{i,x}]^{\mathrm{T}} \\ \boldsymbol{\sigma}_{i,y} = [K_{i,y}, \Delta k_{i,y}]^{\mathrm{T}} \end{cases} \tag{20}$$

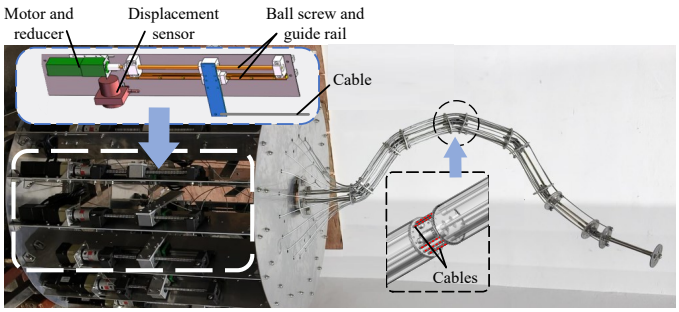

Fig. 3. The developed manipulator platform.

TABLE I

THE DEVELOPED PLATFORM PARAMETERS.

Items	Value	Unit
Single link size	$\phi 60 \times 220$	mm
Total mass of manipulator	1.2	kg
Load capability	0.8	kg
Number of joints and degrees of freedom	5 joints/10-*DOF*	
Joint angle limitation	$[-\pi/6, \pi/6]$	rad
Elastic modulus of cables E	12.5	GPa

2) End stiffness ellipse: for the end stiffness matrix $\boldsymbol{K}_x^{6\times6}$, the main concern is the relationship between the end force $\boldsymbol{F}_d$ and the $\boldsymbol{d}$ translation deformation, which is as follows:

$$\boldsymbol{F}_d = \boldsymbol{K}_{fd} \cdot \boldsymbol{d} \tag{21}$$

where $\boldsymbol{F}_d = [F_x, F_y, F_z]^T$, $\boldsymbol{d} = [d_x, d_y, d_z]^T$, and the 3×3 matrix $\boldsymbol{K}_{fd}$ represents the first three rows and first three columns of the matrix $\boldsymbol{K}_x$.

Further, the displacement produced by applying a unit force to the end-effector, this can be described as a stiffness ellipsoid. According to the calculation of the stiffness ellipsoid [19], the short half-axis of the ellipsoid represents the minimum deformation per unit force and the long half-axis represents the maximum deformation per unit force. Meanwhile, the minimum eigenvalue $\lambda_{min}(\boldsymbol{K}_{fd})$ represents the maximum deformation of the end when it is subjected to a unit force. Therefore, the end stiffness of the manipulator can be visually characterised by the stiffness ellipsoid.

IV. ANALYSIS AND DISCUSSION

In order to analyse the stiffness characteristics of the cable-driven hyper-redundant manipulator, the developed manipulator platform is employed for testing and validation in Fig 3. For the manipulator, the rotational power source is mainly converted into the linear power source by controlling the motor to drive the reducer and ball screw. The ball screw connects the cable to realize the stretching of the cable, and then realizes the movement of the manipulator. The relevant parameters of the manipulator are shown in the Table I.

A. Effect of Cable Tension on Joint Stiffness

With the angle and torque determined, the cable tension needs to be solved in order to calculate the amount of joint

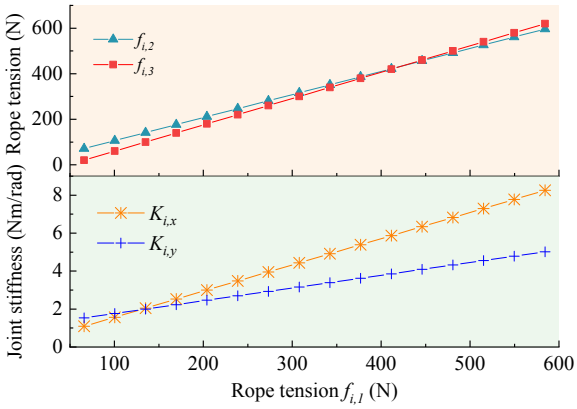

Fig. 4. The variation diagram of cable tensions and joint stiffness.

stiffness. For the single joint structure of the manipulator, three cable drives control two joint angles so that the redundancy is equal to 1. Compared to parallel robots with redundancy greater than 1 [20], the solution of cable tension is relatively simple. Firstly, the set of cable tensions $\boldsymbol{\Omega}$ satisfying the upper and lower ranges can be expressed as:

$$\boldsymbol{\Omega} = \{\boldsymbol{f} \mid f_j \in [f_{\min}, f_{\max}], j = 1, 2, 3\} \tag{22}$$

Meanwhile, the set $\mathbf{P}$ can be used to represent the cable tension distribution that satisfies the static equilibrium condition at the joint.

$$\mathbf{P} = \{\boldsymbol{f} \mid \boldsymbol{\tau} + \boldsymbol{J}_c^T \cdot \boldsymbol{f} = 0\} \tag{23}$$

Therefore, the set of feasible solutions for the multi-group cable tension is denoted as $\boldsymbol{\Lambda} = \boldsymbol{\Omega} \cap \mathbf{P}$. Within the limiting range of cable tensions, the antagonistic forces of the three cables have the same trend and are linearly correlated. The variation of cable tension is set to $\Delta\boldsymbol{f} = [\Delta f_1, \Delta f_2, \Delta f_3]^T$. Combined with (14), it can be inferred that the change of single joint stiffness.

$$\begin{bmatrix} K_{i,x} + \Delta K_{i,x} \\ K_{i,y} + \Delta K_{i,y} \end{bmatrix}^T = diag\left(-\frac{\partial \boldsymbol{J}_c^T}{\partial \boldsymbol{q}} (\boldsymbol{f} + \Delta \boldsymbol{f}) - \boldsymbol{J}_c^T \boldsymbol{K}_l \boldsymbol{J}_c \right) \tag{24}$$

where $\Delta K_{i,x}$, $\Delta K_{i,y}$ denote the stiffness increments of the i-joint rotating along the x-axis and y-axis, respectively. It can be seen that when the cable tensions are varied, the stiffness of the single joint also follows the same trend.

Set the joint angle as $\boldsymbol{q} = [\pi/7, -\pi/9]^T$rad, the joint torque as $\boldsymbol{\tau} = [-1, 0.5]^T$Nm and the upper and lower range of cable tensions as $f \in [20, 600]$N. The multiple sets of cable tension curves and corresponding stiffness curves can be obtained through testing, as shown in Fig. 4. It can be seen that with the change of the a single cable tension, It can be seen that as the tension of the single cable increases, the tensions of the other two cables increase linearly, as well as the joint stiffness.

TABLE II

JOINT STIFFNESS CORRESPONDING TO THE ANGLE LIMIT VALUES.

$\boldsymbol{q}$	$K_{i,x}$	$\Delta k_{i,x}$	$K_{i,y}$	$\Delta k_{i,y}$
$[0,0]^T$	$[1.92, 1.98]$	0.06	$[1.85, 1.90]$	0.05
$[\pi/6, \pi/6]^T$	$[2.96, 7.94]$	4.98	$[2.51, 10.59]$	8.08
$[\pi/6, -\pi/6]^T$	$[2.53, 18.17]$	15.64	$[1.44, 8.18]$	6.74
$[-\pi/6, \pi/6]^T$	$[2.32, 7.50]$	5.18	$[2.17, 10.57]$	8.40
$[-\pi/6, -\pi/6]^T$	$[1.41, 17.05]$	15.64	$[1.37, 8.11]$	6.74

B. Effect of joint angle on Joint Stiffness

In addition to the effect of cable tension on joint stiffness, the Jacobi matrix also affects joint stiffness, which is mainly related to the joint angle. On the one hand, the controllable and intrinsic stiffness in (15) have the existence of Jacobi matrix terms. On the other hand, the solved tension assignments of cable are different when the joint angles are different, which will make the variation range of the joint stiffness to be different.

Considering the coupling relationship between joint angle and stiffness, it is difficult to express it by equations. Therefore, we adjust the joint angle value by numerical calculation to measure the joint stiffness. Through this method, it is analysed the qualitative relationship between the two.

Set the joint torque as $\boldsymbol{\tau} = [0.3, 0.3]^T$Nm, both $q_{i,1}$ and $q_{i,2}$ as between $-\pi/6$ rad and $\pi/6$ rad and the upper and lower range of cable tensions as $f \in [20, 600]$N. By linearly changing the values of $q_{i,1}$ and $q_{i,2}$, the cable tension distribution is solved, and the joint stiffness range is recorded. The heat map of the joint stiffness based on the maximum and minimum values of its variation range is shown in Fig. 5. It can be analyzed that the magnitude of $q_{i,1}$ and $q_{i,2}$ on the whole mainly affects the maximum value of the joint stiffness, which in turn affects the variation range of the joint stiffness. The larger the absolute values of $q_{i,1}$ and $q_{i,2}$, the greater the range of joint stiffness $K_{i,x}$ and $K_{i,y}$ joint stiffness. In addition, it can be seen that positive and negative values of $q_{i,2}$ also affect the range of joint stiffness, as shown in Table II. When $q_{i,2}$ is negative, the range of joint stiffness for $K_{i,x}$ is greater. When $q_{i,2}$ is positive, the range of joint stiffness for $K_{i,y}$ is greater.

C. Effect of Joint Stiffness on End Stiffness

For the manipulator, the end stiffness in static equilibrium affects its actuator operating accuracy. In contrast, the overall configuration of the manipulator in static equilibrium is unchanged, and thus the Jacobi matrix between the joints and the end is fixed. Therefore, according to (19), the main influencing factor of the end stiffness is the joint stiffness. However, for the stiffness of multiple joints, their influence on the end stiffness is different. To analyse the effect of joint stiffness on end stiffness, five joints of the manipulator are controlled for testing. The joint angle is set as $[-\pi/7, -\pi/9, -\pi/9, -\pi/11, \pi/6, \pi/7, \pi/8, -\pi/15, -\pi/12, -\pi/10]^T$rad and the external force is set as $[0, 5, 0, 0, 0, 0]^T$. Combined with (6) (19), the joint torque and the variable stiffness range of each joint can be obtained. In the current

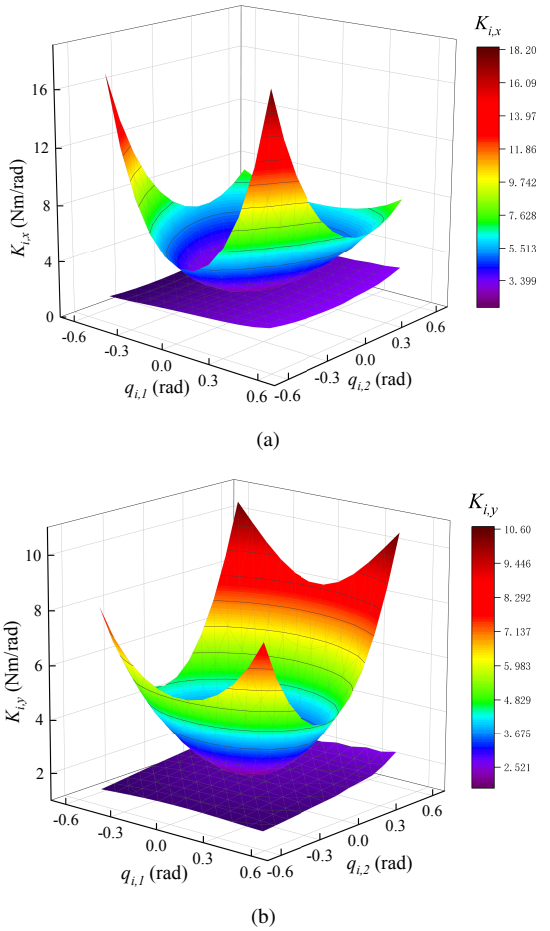

Fig. 5. Heat maps of the limiting values of joint stiffness.

static equilibrium state, the stiffness of different joints is adjusted to change the joint stiffness distribution. Finally, the end stiffness matrix obtained from the solution is recorded and compared visually using the end stiffness ellipse as an evaluation metric, as shown in Fig. 6(a).

In conjunction with the above analysis, the greater the joint angle, the greater the variable range of the joint stiffness. Therefore, when increasing the antagonistic force of the cable corresponding to the 3-th joint, the effect on the end stiffness should be greater compared to the other joints, as shown in Fig. 6(b). However, due to the coupling nature of the stiffness matrix, it is difficult to ensure that it has a good effect in all stiffness directions. On the contrary, for joints with a smaller variable stiffness range, it is possible to have a better effect in one stiffness direction (such as 5-th joint), as shown in the Fig. 6(c). Meanwhile, if the 3-th joint and 5-th joint are added at the same time, they can complement each other in the stiffness directions, as shown in Fig. 6(d). Therefore, changes in overall stiffness or stiffness in a certain direction can be achieved by optimising the distribution of joint stiffness in the same structure.

In addition, the coupling of the end stiffness matrix is mainly related to the Jacobi matrix, so the effect of variable stiffness can also be achieved by changing the configuration of the manipulator. This approach essentially compares the

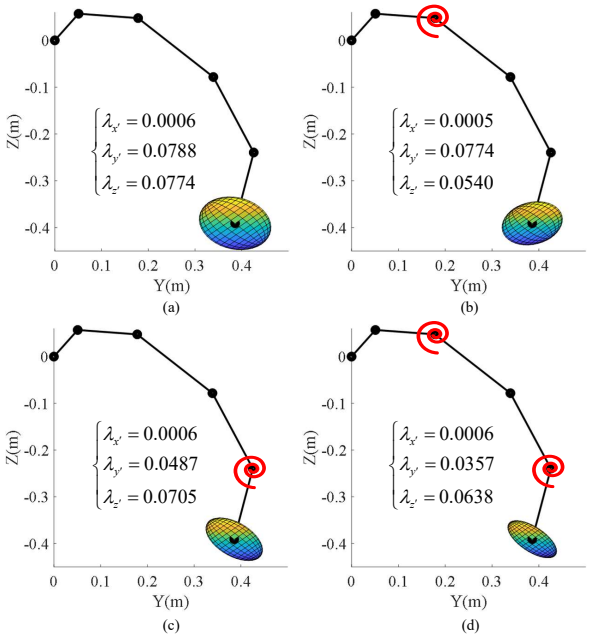

Fig. 6. End stiffness ellipsoids under the stiffness of different joints.

difference of joint angles on end stiffness in different configurations. With the known effect of joint angles on joint stiffness, it is essentially the same as comparing the stiffness of different joint in the same configuration. Therefore, the effect remains the same on the end stiffness analysis.

In summary, the following conclusions can be obtained: 1) For joint stiffness, adjusting the distribution of cable tension can achieve joint variable stiffness. The greater the cable tension, the greater the joint stiffness. However, it is still necessary to keep its cable tension away from the limit value to ensure stability when changing the stiffness; 2) The joint angle also affects the range of joint variable stiffness, the larger the joint angle, the larger the adjustable range of joint stiffness. Meanwhile, the positive and negative values of the joint angle may also affect the range of joint variable stiffness; 3) End stiffness is more easily affected by joint stiffness with a larger adjustable range. By cooperating with the stiffness adjustment of different joints, the end stiffness can be optimized in a single direction or even the overall, thereby improving the performance of the end variable stiffness.

V. CONCLUSIONS

In this paper, we propose an approach to study the joint-to-end variable stiffness characteristics for cable-driven hyper-redundant manipulator. The static models of cable-joint and joint-end are respectively constructed to decouple the whole manipulator system. Meanwhile, the expressions for joint and end stiffness are then derived from the static models, which are used to analyse the main factors affecting them. Finally, combined with platform validation and numerical method, it is found that the joint variable stiffness can be realized by adjusting the cable tension distribution and joint angle. Additionally, the stiffness adjustment and coordination of different joints can make the end stiffness variable. Through these analyses, the theoretical basis can be provided for the subsequent variable stiffness control for cable-driven hyper-redundant manipulator, which can be our future researching directions.

REFERENCES

[1] Z. Mu *et al.*, "Hyper-redundant manipulators for operations in confined space: typical applications, key technologies, and grand challenges," *IEEE Trans. Aerosp. Electron. Syst.*, vol. 58, no. 6, pp. 4928–4937, Dec. 2022.

[2] H. Xu, X. Li, Y. Li, D. Meng, and X. Wang, "Stiffness modeling and dynamics Co-modeling for space cable-driven linkage continuous manipulators," *Mathematics*, vol. 11, no. 8, p. 1874, Jan. 2023.

[3] Q. Chen, M. Li, H. Wu, W. Liu, and J. Peng, "Design, self-calibration and compliance control of modular cable-driven snake-like manipulators," *Mech. Mach. Theory*, vol. 193, p. 105562, Mar. 2024.

[4] J. Lai, B. Lu, and H. K. Chu, "Variable-Stiffness Control of a Dual-Segment Soft Robot Using Depth Vision," *IEEE/ASME Trans. Mechatron.*, vol. 27, no. 2, pp. 1034–1045, Apr. 2022.

[5] L. Zhang *et al.*, "A convolutional dynamic-jerk-planning algorithm for impedance control of variable-stiffness cable-driven manipulators," *Mathematics*, vol. 13, no. 11, p. 2021, Nov. 2022.

[6] A. Zhakatayev, M. Rubagotti, and H. A. Varol, "Energy-aware optimal control of variable stiffness actuated robots," *IEEE Rob. Autom. Lett.*, vol. 4, no. 2, pp. 330–337, Apr. 2019.

[7] A. E. H. Martin, A. M. Sundaram, W. Friedl, V. R. Garate, and M. A. Roa, "Task-oriented stiffness setting for a variable stiffness hand," in *Proc. IEEE Int. Conf. Robot. Automat.*, May 2023, pp. 10275–10281.

[8] X. Gao, X. Li, C. Zhao, L. Hao, and C. Xiang, "Variable stiffness structural design of a dual-segment continuum manipulator with independent stiffness and angular position," *Rob. Comput. Integr. Manuf.*, vol. 67, p. 102000, Feb. 2021.

[9] D. Bruder, M. A. Graule, C. B. Teeple, and R. J. Wood, "Increasing the payload capacity of soft robot arms by localized stiffening," *Sci. Rob.*, vol. 52, no. 10, pp. 6222–6234, Aug. 2023.

[10] K. Yang, C. Chen, Y. Ding, K. Wu, G. Zhang, and G. Yang, "Stiffness modeling and distribution of a modular cable-driven human-like robotic arm," *Mech. Mach. Theory*, vol. 180, p. 105150, Feb. 2023.

[11] H. Jeon *et al.*, "Towards a snake-like flexible robot with variable stiffness using an SMA spring-based friction change mechanism," *IEEE Rob. Autom. Lett.*, vol. 7, no. 3, pp. 6582–6589, July 2022.

[12] Z. Xing, F. Wang, Y. Ji, D. McCoul, X. Wang, and J. Zhao, "A structure for fast stiffness-variation and omnidirectional-steering continuum manipulator," *IEEE Rob. Autom. Lett.*, vol. 6, no. 2, pp. 755–762, Apr. 2021.

[13] Z. Cui and X. Tang, "Analysis of stiffness controllability of a redundant cable-driven parallel robot based on its configuration," *Mechatronics*, vol. 75, p. 102519, May 2021.

[14] J. Yu, J. Tao, G. Wang, X. Li, and H. Wang, "Research on stiffness control of a redundant cable-driven parallel mechanism," *J. Mech. Sci. Technol.*, vol. 36, no. 11, pp. 5735–5743, Nov. 2022.

[15] H. Yuan, W. Zhang, Y. Dai, and W. Xu, "Analytical and numerical methods for the stiffness modeling of cable-driven serpentine manipulators," *Mech. Mach. Theory*, vol. 156, p. 104179, Feb. 2021.

[16] H. Gu, C. Wei, Z. Zhang, and Y. Zhao, "Theoretical and experimental study on active stiffness control of a two-degrees-of-freedom rope-driven parallel mechanism," *J. Mech. Rob.*, vol. 13, no. 1, p. 11018, Feb. 2021.

[17] L. Zhang, Y. Gao, Z. Mu, L. Yan, Z. Li, and M. Gao, "A Variable-Stiffness Planning Method Considering Both the Overall Configuration and Cable Tension for Hyper-Redundant Manipulators," *IEEE/ASME Trans. Mechatron.*, vol. 29, no. 1, pp. 659-667, Feb. 2024.

[18] A. Ajoudani, N. G. Tsagarakis, and A. Bicchi, "Choosing poses for force and stiffness control," *IEEE Trans. Rob.*, vol. 33, no. 6, pp. 1483–1490, Dec. 2017.

[19] J. Zhao, Y. Duan, B. Xie, and Z. Zhang, "FSW robot system dimensional optimization and trajectory planning based on soft stiffness indices," *J. Manuf. Processes*, vol. 63, pp. 88–97, Mar. 2021.

[20] H. Gao *et al.*, "Tension distribution algorithm based on graphics with high computational efficiency and robust optimization for two-redundant cable-driven parallel robots," *Mech. Mach. Theory*, vol. 172, p. 104739, June 2022.